LETTER

doi:10.1038/nature12936

Site- and energy-selective slow-electron production through intermolecular Coulombic decay

Kirill Gokhberg[1], Přemysl Kolorenč[2], Alexander I. Kuleff[1] & Lorenz S. Cederbaum[1]

Irradiation of matter with light tends to electronically excite atoms and molecules, with subsequent relaxation processes determining where the photon energy is ultimately deposited and electrons and ions produced. In weakly bound systems, intermolecular Coulombic decay[1] (ICD) enables very efficient relaxation of electronic excitation through transfer of the excess energy to neighbouring atoms or molecules that then lose an electron and become ionized[2–9]. Here we propose that the emission site and energy of the electrons released during this process can be controlled by coupling the ICD to a resonant core excitation. We illustrate this concept with *ab initio* many-body calculations on the argon–krypton model system, where resonant photoabsorption produces an initial or 'parent' excitation of the argon atom, which then triggers a resonant-Auger-ICD cascade that ends with the emission of a slow electron from the krypton atom. Our calculations show that the energy of the emitted electrons depends sensitively on the initial excited state of the argon atom. The incident energy can thus be adjusted both to produce the initial excitation in a chosen atom and to realize an excitation that will result in the emission of ICD electrons with desired energies. These properties of the decay cascade might have consequences for fundamental and applied radiation biology and could be of interest in the development of new spectroscopic techniques.

Since its prediction[1] in 1997, ICD has been successfully investigated in a variety of systems[7]. It usually proceeds on a femtosecond timescale and becomes faster the more neighbours are present, often dominating most of the competing relaxation processes. ICD remains effective over considerable interatomic distances: in He dimers, the weakest bound systems known in nature, it is operative over distances of about 45 times the atomic radius[8,9]. The initial electronic excitation triggering ICD may be produced directly by photoabsorption, electron impact or even ion impact, as demonstrated recently[10]. It can also result from multistage processes such as Auger decay[11–13], with the overall Auger-ICD cascade initiated by core ionization of an atom (typically through X-ray absorption) that is part of a more complex system. In this case, however, there is little control over where exactly the Auger decay is triggered and where the subsequent ICD takes place. Indeed, in a polyatomic system, all atoms with core-ionization potentials below the energy of the impacting photon may become ionized and undergo an Auger transition.

Our proposal for realizing ICD with control over both the location of the process and the energies of the emitted ICD electrons exploits resonant Auger decay[14]. It uses photons with an energy just below the core-ionization threshold of a selected atom in a larger system, so that at a number of discrete energies the core electron will resonantly absorb the photon and be promoted to some bound, unoccupied orbital to give a highly energetic, core-excited state that can decay through the emission of an Auger electron. In this process, a valence electron fills the initial vacancy and another valence electron is ejected into the continuum, while the initially excited electron remains a spectator. This 'spectator resonant Auger' mechanism produces highly excited valence-ionized states (known as photoionization satellite states). The alternative, 'participator', process, in which the initially excited electron participates in the decay, is usually the much less efficient de-excitation pathway of core excitations.

As sketched in Fig. 1, the resonant Auger decay transforms the initially core-excited species into an excited, valence-ionized state with an excess energy of typically a few tens of electronvolts; the latter can then transfer its excess energy to the environment by continuing to decay electronically through ICD. In contrast to Auger-driven ICD, this resonant-Auger-driven ICD (RA–ICD) offers control over key features of the ICD process. First, in a given environment, the energy of emitted ICD electrons depends sensitively on the energies and populations of the states produced by resonant Auger decay, which in turn depend on the nature of the parent, core-excited state. This offers the possibility of varying the energetic composition of the ICD spectra in a controlled manner by adjusting the energy of the initiating, high-energy photon to resonantly excite the particular parent state that will produce the desired ICD electrons. Second, the initial parent core excitation can be placed selectively not only on chemically different atoms but also on identical atoms occupying non-equivalent sites in the system. (This selectivity stems from the different chemical shifts the atoms experience in different chemical environments and is used in near edge X-ray absorption fine structure spectroscopy to study, for example, the bonding in biologically relevant organic molecules[15].) And because the resonant Auger decay tends to be local and to populate excited valence-ionized states with two holes localized predominantly on the atom bearing the initial excitation[16], the subsequent ICD will mostly ionize the environment in the vicinity of the parent core excitation (Fig. 1b). In other words, the site where the ICD electrons are produced can be selectively chosen.

We illustrate the RA–ICD cascade for ArKr, a simple system that allows for a particularly clear illustration of the processes involved. Here RA–ICD can be initiated using a photon energy of 246.51 eV selectively to populate the $2p_{1/2}^{-1}4s$ state of Ar (ref. 17), which lives for only 5.5 fs (ref. 18) and locally undergoes spectator Auger decay populating a band of excited states of Ar^+ (Methods). These excited valence-ionized states lie between 17 and 22 eV above the ground state of Ar^+ and can therefore undergo ICD with the neighbouring Kr, whose lowest ionization potential is 14 eV. The ICD rates determined from extensive *ab initio* many-body calculations confirm that the ionic states indeed further decay by ICD, with the calculated electron spectrum (Fig. 2a) exhibiting a pronounced peak between 0 and 1 eV and a weaker peak between 2 and 4 eV (see Methods for details of the computational scheme). Following the ICD, Ar^+ and Kr^+ will repel each other, resulting in a dissociation process known as a Coulomb explosion, which endows the ions with ~3.7 eV of kinetic energy.

On increasing the energy of the X-ray photon by just 0.4 eV to 246.93 eV, the $2p_{3/2}^{-1}3d$ parent state of Ar is excited. The resonant Auger decay of this core excitation populates a completely different band of excited states of Ar^+, but these can also all decay further by ICD (Methods). In this case, the spectrum of the emitted electrons (Fig. 2b) consists of one peak between 3 and 5 eV and another between 6 and 8 eV. We see that two different core excitations of the same atom result in very different

[1]Theoretische Chemie, Physikalisch-Chemisches Institut, Universität Heidelberg, Im Neuenheimer Feld 229, 69120 Heidelberg, Germany. [2]Institute of Theoretical Physics, Faculty of Mathematics and Physics, Charles University in Prague, V Holešovičkách 2, 180 00 Prague, Czech Republic.

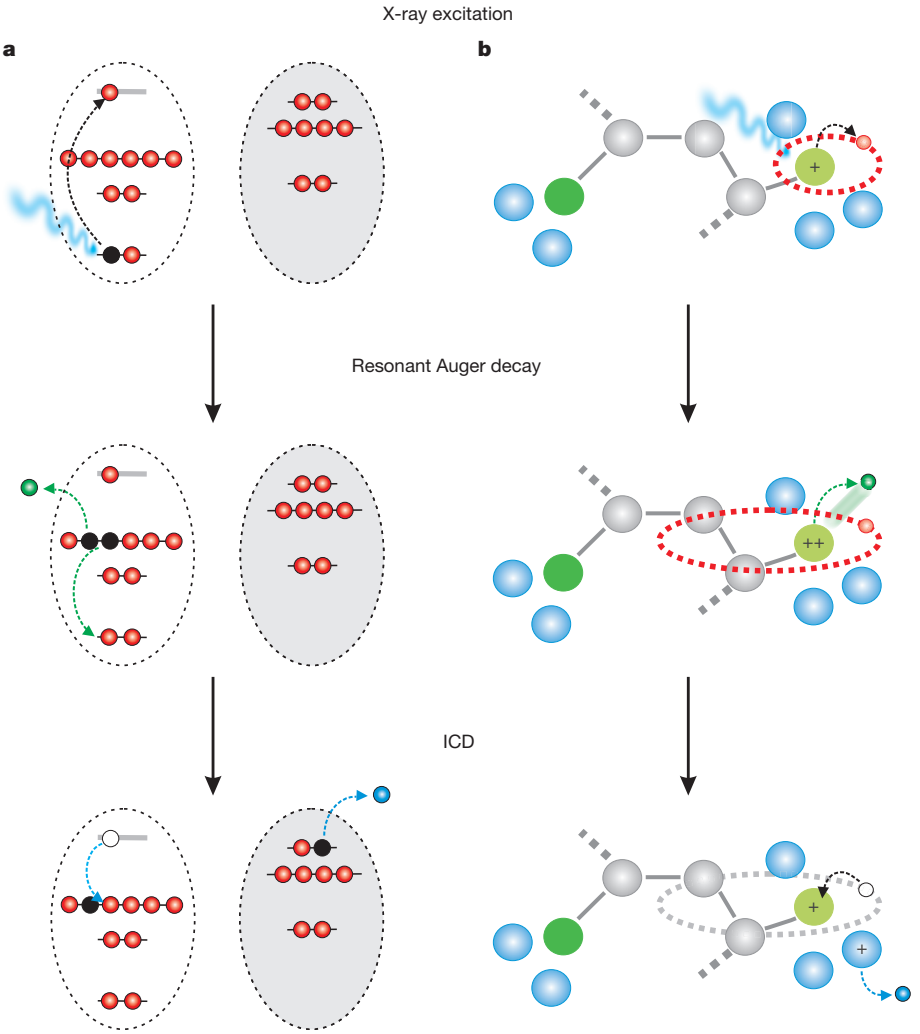

Figure 1 | Schematic illustration of the RA–ICD cascade. a, The mechanism. A parent core-excited state embedded in the environment decays locally by the spectator resonant Auger process, producing highly excited valence-ionized states. These states continue to decay by ICD, ionizing the neighbours in the environment. The two cations produced by ICD repel each other and undergo a Coulomb explosion (not shown). **b**, Selectivity property. The parent state is produced selectively in a given atom of the embedded system. The excited valence-ionized states formed in the resonant Auger process tend to be localized at the site of the initial excitation and decay by ICD, ionizing predominantly neighbours from the environment nearest to this site.

energy distributions of the emitted ICD electrons, illustrating the potential to control the energies of the ICD electrons. We note that in both excitation schemes, only a fraction of a percent of the total decay rate[19] is accounted for by the participator Auger channel, which does not result in ICD; in contrast, the spectator Auger final states, which do undergo further ICD, comprise about 75% of the total population in the case of the $2p_{1/2}^{-1}4s$ parent excitation and more than 95% in the case of the $2p_{3/2}^{-1}3d$ parent excitation. In other systems, such as the molecular dimers experimentally shown to undergo RA–ICD in the companion paper to this one[20], these and other details may of course differ; but the basic underlying mechanism of the RA–ICD cascade will be similar to what we have shown for ArKr.

The ability to control the location and energies of ICD electrons by core-exciting selected atoms to different parent states suggests that the RA–ICD cascade could serve as the foundation for a promising analytical technique. Intriguing possibilities may arise from the fact that the method combines intramolecular Auger decay, which produces Auger electrons that can be used to study the electronic structure of the molecule at the excitation site, with intermolecular, neighbour-involving ICD, which produces electrons that can be used to probe the local environment (Fig. 1b). In the latter regard, RA–ICD may seem similar to the multi-atom resonant photoemission effect suggested to be sensitive to the local chemical environment of an atom in a crystal[21]. Although that effect is also initiated by a core excitation, it involves a single interatomic de-excitation step that results in core-electron emission from a neighbouring atom. But this interatomic decay mode is strongly suppressed[22] and is thus difficult to use, owing to the strong competition of the resonant Auger process in the primary excited atom. In contrast, the final ICD step of the RA–ICD cascade in atomic systems has no competitor (except for the much slower radiative decay) and the whole process is extremely efficient. Even in molecular systems, where additional relaxation modes involving nuclear dynamics are present, the ICD process remains very effective[2,20].

In closing, we note that radiation-induced DNA damage is generally attributed to electrons with energies less than 500 eV (ref. 23) and to radical species[24]. Some radiotherapy approaches incorporate high-atomic-number elements as Auger-electron emitters[25,26] into DNA, for the targeted production of genotoxic electrons thought to arise from the local Auger cascade in the high-atomic-number element. However, a large number of interatomic decay channels will be open in a high-atomic-number Auger-electron emitter placed in an environment as complex as DNA and its solvation shell. Indeed, the probability of ICD-like processes[27,28] taking place in this system and simultaneously generating genotoxic electrons and radical cations will be very high and ought to be considered (Methods). We also note that the RA–ICD cascade is more efficient and selective in producing genotoxic species than are traditional

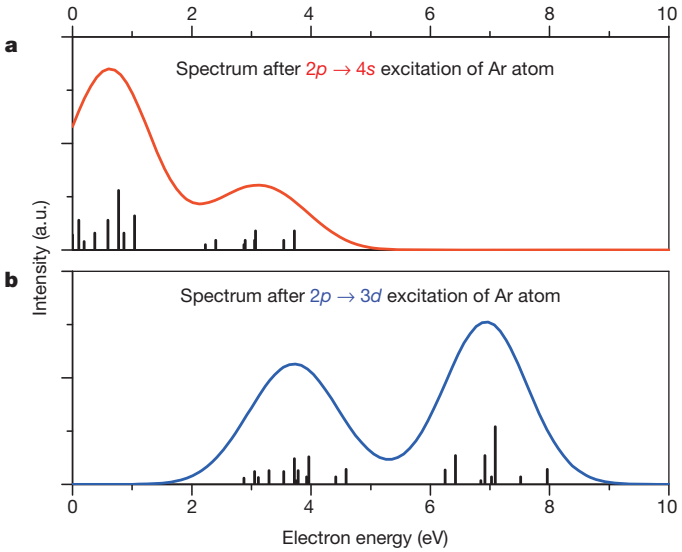

Figure 2 | Spectra of the ICD electrons emitted in the RA–ICD cascades in ArKr. ICD electron spectra for core excitation of the $Ar(2p_{1/2}^{-1}4s)$ parent state at 246.51 eV (**a**) and core excitation of the $Ar(2p_{3/2}^{-1}3d)$ parent state at 246.93 eV (**b**). The discrete lines are obtained using the frozen-nuclei approximation, whereas the continuous lines are evaluated by the convolution of each discrete line with a Gaussian with a full-width at half-maximum of 1.4 eV, qualitatively accounting for the nuclear dynamics (see Methods for computational details). The spectra illustrate that two different core excitations of the same atom lead to very different energy distributions of the ICD electrons. a.u., arbitrary units.

photon-activated techniques that initiate the Auger cascade through K-shell ionization[26]. In particular, the site- and energy-selectivity of the resonant core excitation process make it possible to tune the energies of the slow electrons generated. This feature might prove useful in optimizing radiotherapy efficiency. It has been shown[29,30] that electrons with energies between 0 and 4 eV predominantly induce single-strand breaks in DNA, and that the more damaging double-strand breaks are more efficiently produced by electrons with energies greater than 6 eV. We believe that a detailed mechanistic understanding of DNA lesions, in conjunction with the tunability of RA–ICD, could offer enough control over radiation-induced cell damage to lead to efficient cancer therapies.

METHODS SUMMARY

The ICD lifetimes of the involved states were computed using an *ab initio* many-body method. This method is based on the general Fano resonance formalism, in which the initial decaying state is represented as a bound (discrete) state embedded in the continuum of final states of the decay. The $\mathcal{L}^2$ approximations for the discrete and continuum components of the $(N-1)$-electron wavefunction are obtained within the Green's function in the algebraic diagrammatic construction (ADC) approach, and the resulting discretized spectrum is renormalized and interpolated in energy using the Stieltjes imaging technique. The potential energy curves of the initial and final ICD states were modelled using atomic data. The final ICD-electron spectra were obtained by convolving the discrete electronic transitions with an appropriate Gaussian profile.

Online Content Any additional Methods, Extended Data display items and Source Data are available in the online version of the paper; references unique to these sections appear only in the online paper.

Received 7 May 2012; accepted 28 November 2013.
Published online 22 December 2013.

1. Cederbaum, L. S., Zobeley, J. & Tarantelli, F. Giant intermolecular decay and fragmentation of clusters. *Phys. Rev. Lett.* **79,** 4778–4781 (1997).
2. Jahnke, T. *et al.* Ultrafast energy transfer between water molecules. *Nature Phys.* **6,** 139–142 (2010).
3. Mucke, M. *et al.* A hitherto unrecognized source of low-energy electrons in water. *Nature Phys.* **6,** 143–146 (2010).
4. Grieves, G. A. & Orlando, T. M. Intermolecular Coulomb decay at weakly coupled heterogeneous interfaces. *Phys. Rev. Lett.* **107,** 016104 (2011).
5. Schwartz, C. P., Fatehi, S., Saykally, R. J. & Prendergast, D. Importance of electronic relaxation for inter-Coulombic decay in aqueous systems. *Phys. Rev. Lett.* **105,** 198102 (2010).
6. Stoychev, S. D., Kuleff, A. I. & Cederbaum, L. S. Intermolecular Coulombic decay in small biochemically relevant hydrogen-bonded systems. *J. Am. Chem. Soc.* **133,** 6817–6824 (2011).
7. Hergenhahn, U. Interatomic and intermolecular Coulombic decay: the early years. *J. Electron Spectrosc. Relat. Phenom.* **184,** 78–90 (2011).
8. Sisourat, N. *et al.* Ultralong-range energy transfer by interatomic Coulombic decay in an extreme quantum system. *Nature Phys.* **6,** 508–511 (2010).
9. Havermeier, T. *et al.* Interatomic Coulombic decay following photoionization of the helium dimer: observation of vibrational structure. *Phys. Rev. Lett.* **104,** 133401 (2010).
10. Kim, H. K. *et al.* Enhanced production of low energy electrons by alpha particle impact. *Proc. Natl Acad. Sci. USA* **108,** 11821–11824 (2011).
11. Santra, R. & Cederbaum, L. S. Coulombic energy transfer and triple ionization in clusters. *Phys. Rev. Lett.* **90,** 153401 (2003).
12. Morishita, Y. *et al.* Experimental evidence of interatomic Coulombic decay from the Auger final states in argon dimers. *Phys. Rev. Lett.* **96,** 243402 (2006).
13. Yamazaki, M. *et al.* Decay channel dependence of the photoelectron angular distributions in core-level ionization of Ne dimers. *Phys. Rev. Lett.* **101,** 043004 (2008).
14. Ueda, K. Core excitation and de-excitation spectroscopies of free atoms and molecules. *J. Phys. Soc. Jpn* **75,** 032001 (2006).
15. Feyer, V. *et al.* Core level study of alanine and threonine. *J. Phys. Chem. A* **112,** 7806–7815 (2008).
16. Hergenhahn, U. *et al.* The resonant Auger spectra of formic acid, acetaldehyde, acetic acid and methyl formate. *Chem. Phys.* **289,** 57–67 (2003).
17. de Gouw, J. A., van Eck, J., Peters, A. C., van der Weg, J. & Heideman, H. G. M. Resonant Auger spectra of the $2p^{-1}nl$ states of argon. *J. Phys. B* **28,** 2127–2141 (1995).
18. Fuggle, J. C. & Alvarado, S. F. Core-level lifetimes as determined by X-ray photoelectron spectroscopy measurements. *Phys. Rev. A* **22,** 1615–1624 (1980).
19. Gorczyca, T. W. & Robicheaux, F. Auger decay of the photoexcited $2p^{-1}nl$ Rydberg series in argon. *Phys. Rev. A* **60,** 1216–1225 (1999).
20. Trinter, F. *et al.* Resonant Auger decay driving intermolecular Coulombic decay in molecular dimers. *Nature* http://dx.doi.org/10.1038/nature12927 (this issue).
21. Kay, A. *et al.* Multi-atom resonant photoemission: a method for determining near-neighbor atomic identities and bonding. *Science* **281,** 679–683 (1998).
22. Carravetta, V. & Ågren, H. An ab initio method for computing multi-atom resonant photoemission. *Chem. Phys. Lett.* **354,** 100–108 (2002).
23. Pomplun, E. A new DNA target model for track structure calculations and its first application to I-125 Auger electrons. *Int. J. Radiat. Biol.* **59,** 625–642 (1991).
24. von Sonntag, C. *Free-Radical-Induced DNA Damage and Its Repair* (Springer, 2006).
25. Adelstein, J. S., Kassis, A. I., Bodei, L. & Mariani, G. Radiotoxicity of iodine-125 and other Auger-electron-emitting radionuclides: background to therapy. *Cancer Biother. Radiopharm.* **18,** 301–316 (2003).
26. Fairchild, R. G., Brill, A. B. & Ettinger, K. V. Radiation enhancement with iodinated deoxyuridine. *Invest. Radiol.* **17,** 407–416 (1982).
27. Aziz, E. F., Ottosson, N., Faubel, M., Hertel, I. V. & Winter, B. Interaction between liquid water and hydroxide revealed by core-hole de-excitation. *Nature* **455,** 89–91 (2008).
28. Pokapanich, W. *et al.* Ionic-charge dependence of the intermolecular Coulombic decay time-scale for aqueous ions probed by the core-hole clock. *J. Am. Chem. Soc.* **133,** 13430–13436 (2011).
29. Boudaïffa, B., Cloutier, P., Hunting, D., Huels, M. A. & Sanche, L. Resonant formation of DNA strand breaks by low-energy (3 to 20 eV) electrons. *Science* **287,** 1658–1660 (2000).
30. Martin, F. *et al.* DNA strand breaks induced by 0–4 eV electrons: the role of shape resonances. *Phys. Rev. Lett.* **93,** 068101 (2004).

Acknowledgements The research leading to these results received funding from the European Research Council under the European Community's Seventh Framework Programme (FP7/2007-2013)/ERC Advanced Investigator Grant no. 227597. P.K. acknowledges the support from the Czech Science Foundation (grant no. P208/12/0521).

Author Contributions K.G., A.I.K. and L.S.C. had the idea for the cascade mechanism and its potential consequences. P.K. computed the lifetimes, and K.G. and A.I.K. evaluated the electronic spectra. K.G., A.I.K. and L.S.C. wrote the paper.

Author Information Reprints and permissions information is available at www.nature.com/reprints. The authors declare no competing financial interests. Readers are welcome to comment on the online version of the paper. Correspondence and requests for materials should be addressed to K.G. (kirill.gokhberg@pci.uni-heidelberg.de) or A.I.K. (alexander.kuleff@pci.uni-heidelberg.de).

METHODS

Identifying open ICD channels. After the excited valence-ionized states of ArKr have been populated by resonant Auger decay of the $2p_{1/2}^{-1}4s$ or $2p_{3/2}^{-1}3d$ parent excitation of Ar, they can further decay by ICD that can be identified in the following simple way.

As the parent excitation and the following resonant Auger process are ultrafast (the resonant-Auger lifetime in the studied cases is only 5.5 fs (ref. 18)), the Auger transitions take place at equilibrium internuclear distance of the neutral system, $R_{eq} = 3.88$ Å. Therefore, the states that can further decay by ICD are those whose energies at around R_{eq} are larger than the energies of the final Ar^+Kr^+ states of the ICD process. To determine the relevant energies at around R_{eq}, we first make use of the fact that bound excited valence-ionized states of van der Waals dimers are known to be very shallow, having dissociation energies in the millielectronvolt range[31]. Therefore, the potential energy curves of the $Ar^+(3p^{-2}nl)Kr$ states can be well approximated by horizontal lines calibrated to the corresponding $Ar^+(3p^{-2}nl)$ energies. In contrast, the Coulomb repulsion between the two ions in the final Ar^+Kr^+ states of ICD determines the $1/R$ asymptotic behaviour of the corresponding potential energy curves. As shown in our previous studies[32,33], analytical curves based on the Coulomb law and calibrated at infinite internuclear distance to the sum of the energies of the corresponding atomic fragments[34] give reliable values for the energies of these states around R_{eq}.

In Extended Data Fig. 1, we depict the energy diagram of the excited valence-ionized states of ArKr most populated in the resonant Auger decay of the $2p_{1/2}^{-1}4s$ parent state together with all possible final ICD states. From the plot, it becomes obvious that apart from the $Ar^+(3p^{-2}(^3P)4s)Kr$ state, all other excited valence-ionized states depicted in the graph can decay by ICD around R_{eq}. The figure also gives the relative populations of the final Auger states[17] (in per cent).

Increasing the energy of the X-ray photon by just 0.4 eV would excite the $2p_{3/2}^{-1}3d$ parent state at 246.93 eV. The resonant Auger decay of this core excitation populates a totally different band of excited valence-ionized states. Two series of $Ar^+(3p^{-2}nl)Kr$ states are populated by the resonant Auger transition[17]. The $Ar^+(3p^{-2}3d)Kr$ states are produced in the strict spectator transition with the excited electron still occupying the $3d$ orbital. In addition, the resonant Auger decay strongly populates the 'shake-up satellite' $Ar^+(3p^{-2}4d)Kr$ states, where the excited spectator electron is promoted to the higher lying $4d$ orbital. The energy diagram of these states together with the final Ar^+Kr^+ states populated by the ICD is shown in Extended Data Fig. 2. We see that all the excited valence-ionized states produced by the resonant Auger process can further decay by ICD around R_{eq}.

Evaluation of the ICD rates. To see whether the ICD is an operative mode of relaxation of these ionized excited states, we need to compute the ICD rates or, equivalently, the ICD lifetimes. For the evaluation of the ICD lifetimes, we used an *ab initio* many-body approach. The method is well documented in the literature[35] and is based on the general Fano resonance formalism[36], in which the initial decaying state is represented as a bound (discrete) state embedded in and interacting with the continuum of final states of the decay. The $\mathcal{L}^2$ approximations for the discrete and continuum components of the $(N-1)$-electron wavefunction are obtained within the Green's function in the ADC approach[37], and the resulting discretized spectrum is renormalized and interpolated in energy using the Stieltjes imaging technique[38]. The Green's function calculations were performed using large basis sets. Both effective core potential ECP.Dolg.6s6p3d1f.4s4p3d1f.8e-MWB (ref. 39) and standard Dunning aug-cc-pVQZ (refs 40, 41) basis sets with additional diffuse and distributed functions were used as an input data, giving very similar results for the lifetimes.

Each state produced by resonant Auger decay and decaying by ICD has been found to have its own individual lifetime. The ICD lifetimes of the various $Ar^+(3p^{-2}4s)Kr$ and $Ar^+(3p^{-2}3d)Kr$ decaying states were found to be between 13 and 220 fs, and the lifetimes of the shake-up $Ar^+(3p^{-2}4d)Kr$ satellites are between 600 fs and 2 ps. We see that indeed the ICD is efficient and will be the primary relaxation mode of the states produced by the resonant Auger transition. This is also confirmed by the recent measurements[20] of the RA–ICD cascade in $(N_2)_2$ and $(CO)_2$ showing that the ICD takes place before the excited molecule is able to undergo dissociation, suggesting a timescale of <10 fs for the ICD process. Notably, the ICD rate strongly increases with the increase of the number of neighbours[42,43], making the ICD in larger clusters, as well as in biological media, an extremely efficient mode of relaxation.

ICD electron spectra after RA–ICD cascade in ArKr. From the generally high efficiency of the ICD process, we can estimate the ICD electron spectra assuming that the whole cascade takes place at the equilibrium distance. This assumption is strongly supported by the measurements[20] on the process in N_2 and CO dimers, which show that the whole cascade takes place at the equilibrium distance of the dimer. Within this approximation, the ICD-electron spectrum will consist of discrete lines with positions corresponding to the energy differences between the initial and final states of the ICD process, and heights reflecting the population of the given decaying state and the multiplicity of the final one. For the two studied cases, the ICD-electron spectra obtained in this way have been plotted in Fig. 2. We see that, for the $2p_{1/2}^{-1}4s$ parent state, the spectrum has two peaks: a pronounced peak between 0 and 1 eV and a weaker peak between 2 and 4 eV (Fig. 2a). For the $2p_{3/2}^{-1}3d$ parent state, the spectrum again consists of two peaks but in different energy regions: a peak between 3 and 5 eV and another between 6 and 8 eV (Fig. 2b). Comparing the spectra, we notice that a small change in core-excitation energies leads to totally different energies of electrons emitted in the ICD. In both cases, the final ICD products, Ar^+ and Kr^+, will repel each other, resulting in a Coulomb explosion. At the end of this dissociative process, the ions will acquire a kinetic energy of 3.7 eV. This energy can be directly measured in dimers, resulting in the 'kinetic energy release spectrum'[2]. In the frozen-nuclei approximation, this spectrum would consist of a single line at 3.7 eV. As for the ICD-electron distribution (see below), the nuclear motion will introduce a broadening of this line.

The spectra of discrete lines shown in Fig. 2 reflect only the electronic degrees of freedom. We can take a step further and account for the vibrational broadening that the initial distribution of the positions of the nuclei in the neutral will introduce. This initial distribution is given by a wave packet (essentially a Gaussian) that is centred at R_{eq} and has a width of about 0.4 Å. Therefore, to account for the vibrational broadening, each discrete line in Fig. 2 has to be convolved with a Gaussian with a full-width at half-maximum of 1.4 eV. This value reflects the width of the wave packet (0.4 Å) in the electronic ground state of ArKr. The results of this procedure are shown with continuous lines in the electron spectra in Fig. 2. We note that, despite its simplicity, this procedure for obtaining ICD-electron spectra usually gives reliable results. For instance, the ICD-electron spectrum of a water dimer[44,45] obtained using this procedure is in fairly good agreement with the experimental results[2].

We also note that computing highly accurate ICD electron spectra for the RA–ICD cascade in ArKr is beyond the scope of the present paper. The emphasis here is put on uncovering the potential that this cascade offers for larger systems. The example of ArKr is used only to illustrate the high degree of control with which low-energy electrons (LEE) and radical cations can be produced. Both low-energy electrons and radical cations are known to be important in radiation biology, because they induce DNA lesions.

Additional sources of ICD electrons. Relaxation of a core-excited high-Z element embedded in a biological medium will result in ICD-electron emission in the terminal step of an RA–ICD cascade, but other ICD processes can be a source of additional genotoxic electrons. Here we briefly discuss some of these possibilities, noting that all ICD processes simultaneously produce an ICD electron and a radical cation that both contribute to the DNA damage[24].

One type is core-ICD processes. For Auger cascades taking place in an environment, the emission of Auger electrons is accompanied by the emission of electrons by the core-ICD process, in which the parent excitation decays not in a local Auger cascade step but by interatomically ionizing the environment. Therefore, at each step of the corresponding cascade, the energy release accompanying the core transition on the parent species can either be used to ionize it (Auger process) or be transferred to the environment to ionize a neighbour instead (core-ICD process). The core-ICD process was experimentally observed both after core excitation[27] and after core ionization[28,46], with core ionization of solvated metallic ions shown[46] to follow decay pathways where the core-ICD/Auger branching ratio reaches values as high as 40%. More relevant for the present discussion, the core excitation of OH^-_{aq} was found[27] to relax through the core-ICD process with neighbouring water molecules, with the local Auger decay completely suppressed. This outstanding efficiency of the core-ICD process has been explained[4] by the pronounced overlap between the molecular orbitals located on the parent species and the outer valence orbitals of the water molecules in the solvation shell.

It may also happen that in the Auger cascade in the parent species some Coster–Kronig transitions are energetically forbidden and do not appear in the cascade. In an environment such transitions may, however, become allowed and proceed by ionizing the neighbours. For example, the ionization of $2s$ electron of the isolated Na^+, Mg^{2+} and Al^{3+} ions does not lead to the electronic decay of the resulting states. The energy of the $2p \rightarrow 2s$ transition is not sufficient to remove an additional electron from the ions. In aqueous solutions, new interatomic decay channels open owing to the presence of neighbours, because the energy released in the $2p \rightarrow 2s$ transition is sufficient to ionize the water molecules. By analysing the photoelectron spectra of the hydrated ions, it has been shown[47] that the lifetimes of the respective $2s$ ionized states are between 3 and 1 fs, indicating that the process is, surprisingly, highly efficient. Another relevant observation on high-Z cascades is that the rates of these core-ICD transitions tend to increase with increasing charge on the parent ion[28,47].

A large number of interatomic decay channels will open if a high-Z Auger electron emitter is placed in an environment as complex as DNA and its solvation shell. At each step of the cascade, the probability of a core-ICD process occurring can become considerable owing to the large number of neighbours and the high charge accumulated

on the parent high-Z element. Each Coster–Kronig-like core-ICD transition contributes an additional ICD electron. All together, the total number of ICD electrons in such a cascade can be substantial.

Another possible source of genotoxic electrons is ICD processes triggered by electron impact. It is generally accepted within the radiation biology community that the genotoxic electrons are those with energies below 500 eV (see, for example, ref. 23). Electrons with energies below 15 eV have been shown to generate DNA lesions by means of dissociative electron attachment[29,48], but how electrons with higher energies induce DNA strand breakage remains an open question. A plausible scenario is that these electrons further ionize the environment (water or the DNA itself) and trigger more ICD events, thus producing additional low-energy electrons. Indeed, electron scattering experiments have shown that inner-valence states can be efficiently ionized by electron impact: in the case of water, the ionization cross-section for the inner-valence $2a_1$ orbital by electrons with an incident energy of 250 eV is larger than the cross-section for ionization of all three outer valence orbitals together[49], with experiments indicating that this holds also for other molecules[50]. These inner-valence ionized (or excited) states produced by electron impact can then efficiently decay by ICD ionizing their environment[2], suggesting that the genotoxic effect of high-Z elements used as Auger emitters is at least partly due to follow-up ICD processes initiated by the Auger electrons.

We note that a similar idea has been discussed[51] to explain the effect of secondary electrons with energies above about 35 eV produced by heavy-ion impact, which can efficiently ionize the $2a_1$ orbital of a water molecule in the DNA solvation shell and thereby trigger an ICD process. The resultant simultaneous presence of three slow electrons (secondary, inner-valence ionized and ICD) in the vicinity of a DNA was suggested[51] to be very effective in inducing strand breakages. We therefore conclude that, irrespective of whether energy is deposited in the system by photons, electrons or ions, ICD will be triggered and will contribute to the DNA damage.

31. Hausamann, D. & Morgner, H. The heteronuclear rare gas ions. A simple model for the determination of the potential curves. *Mol. Phys.* **54,** 1085–1099 (1985).
32. Stoychev, S. D., Kuleff, A. I., Tarantelli, F. & Cederbaum, L. S. On the interatomic electronic processes following Auger decay in neon dimer. *J. Chem. Phys.* **129,** 074307 (2008).
33. Demekhin, Ph. V. *et al.* Interatomic Coulombic decay in NeAr following K-LL Auger transition in the Ne atom. *J. Chem. Phys.* **131,** 104303 (2009).
34. National Institute of Standards and Technology. *NIST Atomic Spectra Database* http://physics.nist.gov/asd (2012).
35. Averbukh, V. & Cederbaum, L. S. Ab initio calculation of interatomic decay rates by a combination of the Fano ansatz, Green's-function methods, and the Stieltjes imaging technique. *J. Chem. Phys.* **123,** 204107 (2005).
36. Fano, U. Effects of configuration interaction on intensities and phase shifts. *Phys. Rev.* **124,** 1866–1878 (1961).
37. Schirmer, J., Trofimov, A. B. & Stelter, G. A non-Dyson third-order approximation scheme for the electron propagator. *J. Chem. Phys.* **109,** 4734–4744 (1998).
38. Hasi, A. U. in *Electron-Molecule and Photon-Molecule Collisions* (eds Rescigno, T., McKoy, V. & Schneider, B.) 281–298 (Plenum, 1979).
39. Peterson, K. A., Figgen, D., Goll, E., Stoll, H. & Dolg, M. Systematically convergent basis sets with relativistic pseudopotentials. II. Small-core pseudopotentials and correlation consistent basis sets for the post-d group 16-18 elements. *J. Chem. Phys.* **119,** 11113–11123 (2003).
40. Woon, D. E. & Dunning, T. H. Gaussian basis sets for use in correlated molecular calculations. III. The atoms aluminum through argon. *J. Chem. Phys.* **98,** 1358–1371 (1993).
41. Wilson, A. K., Woon, D. E., Peterson, K. A. & Dunning, T. H. Gaussian basis sets for use in correlated molecular calculations. IX. The atoms gallium through krypton. *J. Chem. Phys.* **110,** 7667–7676 (1999).
42. Santra, R., Zobeley, J. & Cederbaum, L. S. Electronic decay of valence holes in clusters and condensed matter. *Phys. Rev. B* **64,** 245104 (2001).
43. Öhrwall, G. *et al.* Femtosecond interatomic Coulombic decay in free neon clusters: large lifetime differences between surface and bulk. *Phys. Rev. Lett.* **93,** 173401 (2004).
44. Müller, I. B. & Cederbaum, L. S. Ionization and double ionization of small water clusters. *J. Chem. Phys.* **125,** 204305 (2006).
45. Stoychev, S. D., Kuleff, A. I. & Cederbaum, L. S. On the intermolecular Coulombic decay of singly and doubly ionized states of water dimer. *J. Chem. Phys.* **133,** 154307 (2010).
46. Ottosson, N., Öhrwall, G. & Björneholm, O. Ultrafast charge delocalization dynamics in aqueous electrolytes: new insights from Auger electron spectroscopy. *Chem. Phys. Lett.* **543,** 1–11 (2012).
47. Öhrwall, G. *et al.* Charge dependence of solvent-mediated intermolecular Coster-Kronig decay dynamics of aqueous ions. *J. Phys. Chem. B* **114,** 17057–17061 (2010).
48. Huels, M. A., Boudaïffa, B., Cloutier, P., Hunting, D. & Sanche, L. Single, double, and multiple double strand breaks induced in DNA by 3-100 eV electrons. *J. Am. Chem. Soc.* **125,** 4467–4477 (2003).
49. Milne-Brownlie, D. S. *et al.* Dynamics in electron-impact ionization of H_2O. *Phys. Rev. A* **69,** 032701 (2004).
50. McCarthy, I. E. & Weigold, E. Electron momentum spectroscopy of atoms and molecules. *Rep. Prog. Phys.* **54,** 789–879 (1991).
51. Surdutovich, E. & Solov'yov, A. V. Multiscale physics of ion-beam cancer therapy. *J. Phys. Conf. Ser.* **373,** 012001 (2012).

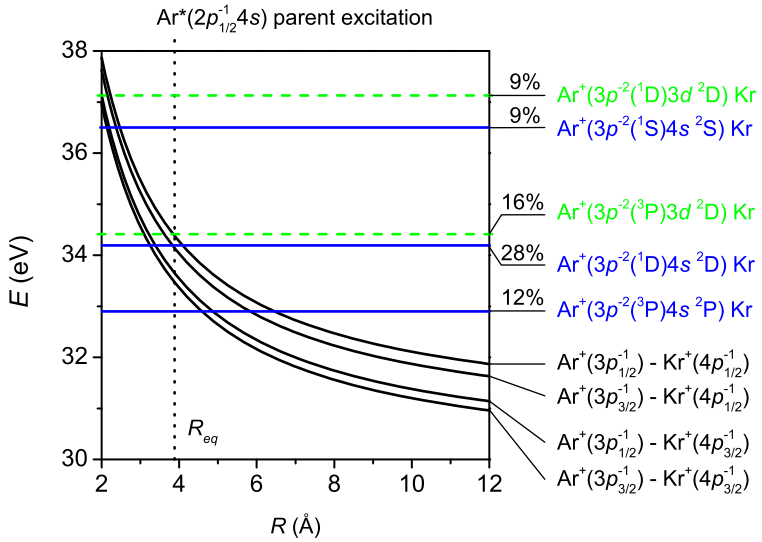

Extended Data Figure 1 | Model potential energy curves of the initial and final ICD states of ArKr produced on excitation at 246.51 eV. The horizontal lines indicate the potential energy curves of the excited valence-ionized states produced through the resonant Auger decay of the parent state following Ar($2p^{-1}_{1/2}4s$) core excitation at 246.51 eV. The steep curves indicate the potential energy of the two-site doubly ionized final states obtained after ICD. The relative populations of the final resonant Auger states are given in per cent. Only states acquiring more than 5% of the total population are depicted. The equilibrium distance of the neutral ArKr (R_{eq} = 3.88 Å) is shown as a vertical dotted line.

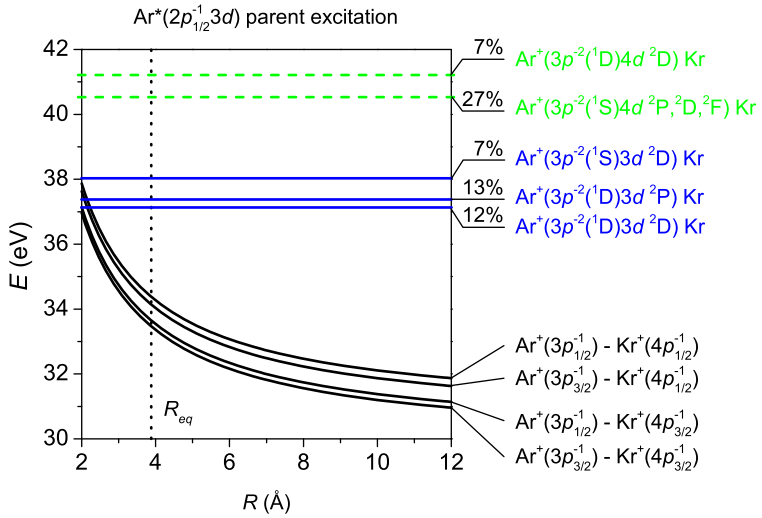

Extended Data Figure 2 | Model potential energy curves of the initial and final ICD states of ArKr produced on excitation at 246.93 eV. The horizontal lines indicate the potential energy curves of the excited valence-ionized states produced through the resonant Auger decay of the parent state following $Ar(2p_{3/2}^{-1}3d)$ core excitation at 246.93 eV. The steep curves indicate the potential energy of the two-site doubly ionized final states obtained after ICD. The relative populations of the final resonant Auger states are given in per cent. Only states acquiring more than 5% of the total population are depicted. The equilibrium distance of the neutral ArKr ($R_{eq} = 3.88$ Å) is shown as a vertical dotted line.